

Interplay of Probabilistic Shaping and the Blind Phase Search Algorithm

Darli A. A. Mello, Fabio A. Barbosa and Jacklyn D. Reis

Abstract—Probabilistic shaping (PS) is a promising technique to approach the Shannon limit using typical constellation schemes. However, the impact of PS on the chain of signal processing algorithms of a coherent receiver still needs further investigation. In this work we study the interplay of PS and phase recovery using the blind phase search (BPS) algorithm, which is currently a de-facto standard in optical communications systems. We first investigate a supervised phase search (SPS) algorithm as a theoretical upper bound on the BPS performance, assuming perfect decisions. It is shown that PS influences the SPS algorithm, but its impact can be alleviated by moderate noise-rejection window sizes. On the other hand, BPS is affected by PS even for long windows because of correlated erroneous decisions in the phase recovery scheme. The simulation results also showed, for investigated constellations, that the capacity-maximizing shaping is near to the worst-case situation for BPS, causing potential implementation penalties.

Index Terms—Coherent optical communications, phase recovery, probabilistic shaping.

I. INTRODUCTION

Probabilistic shaping (PS) is a digital transmission technique by which constellation symbols are transmitted with different a-priori probabilities. In general, symbols with larger amplitudes are transmitted with lower probabilities. PS maximizes the mutual information achieved by the transmission scheme for a given signal constellation and signal to noise ratio (SNR) and allows, in certain conditions, to approach the Shannon limit. Although PS has been known for decades [2], [3], its application on practical systems is still in its infancy. Significant implementation advances have been recently proposed by Böcherer et al. in [4].

In optical systems, the interest in PS has gained significant momentum. To our knowledge, PS has been first addressed in the context of optical communications by Beygi et al. in [5], where a rate-adaptive coded modulation scheme with probabilistic signal shaping has been proposed. The impact of rate adaptive coded-modulation with PS on optical networking has been quantified by Mello et al. in [6]. Yankov et al. investigated in [7] an implementation of PS for turbo codes. The combination of PS with low-density parity-check codes (LDPC) for optical communications has been shown by Fehenberger et al. in [8]. The first experimental demonstration of PS for optical communications has been accomplished by

Buchali et al. in [9], for a 64-QAM modulated signal. Since then, PS has been applied to different contexts, ranging from transoceanic applications [10], [11] to unrepeated optical transmission [12]. PS has already been demonstrated in a large set of experiments, but fully supervised equalization and phase recovery, with controlled conditions, are widely used. One of the first works to relate phase recovery and PS in more practical scenarios has been recently presented by Pilori et al. in [13]. Supervised and partially-supervised pilot-aided phase recovery were investigated. The performance of phase recovery algorithms was assessed from an end-to-end perspective and in particular configurations.

In this paper, we provide a detailed analysis on the interplay of PS and the blind phase search (BPS) algorithm, which is a de-facto standard in optical communications systems. Supervised phase search (SPS), a phase recovery algorithm with the same architecture of BPS, but with perfect decisions, is first investigated by analytical derivations and Monte Carlo simulations. This configuration is used to derive an upper bound on the BPS performance. BPS is only studied by simulations, as the analytical modeling becomes overly complex because of the decision process. The remainder of this paper is divided as follows. Section II presents the PS fundamentals and introduces the basic mathematical model. Section III investigates by analytical modeling and simulations the interplay of PS and SPS. Section IV studies the impact of PS on the BPS algorithm. Lastly, Section V concludes the paper.

II. SYSTEM MODEL

Let the i^{th} constellation symbol s_i be transmitted over a complex additive white Gaussian noise (AWGN) channel. The phase noise associated with the transmitter and local oscillator lasers is expressed by a multiplicative factor $e^{j\theta_n}$, such the received symbol r_i is given by:

$$r_i = s_i e^{j\theta_n} + n'_i \quad (1)$$

where the complex noise term n'_i has zero mean and variance $2\sigma_n^2$. Phase recovery algorithms resort to the fact that θ_n varies slowly over time, such that it is approximately constant over N symbols. In practice, the size of N depends on the linewidth of transmitter and local oscillator lasers.

Probabilistic shaping is usually implemented by applying the Maxwell-Boltzmann distribution to the a-priori probabilities P_m of symbols s_m of the transmitted constellation [2]:

$$P_m = \frac{e^{-\lambda|s_m|^2}}{\sum_{k=1}^M e^{-\lambda|s_k|^2}} \quad (2)$$

D. A. A. Mello and F. A. Barbosa are with the School of Electrical and Computer Engineering, University of Campinas (Unicamp), Campinas, Brazil. J. D. Reis is with Idea! Electronic Systems.

At Unicamp, this work was supported by FAPESP grants 2015/24341-7 and 2015/24517-8. J. Reis was supported by CNPq grant 311871/2016-0. We would like to thank Omar Domingues for the constrained capacity calculations. Part of this work appears in [1].

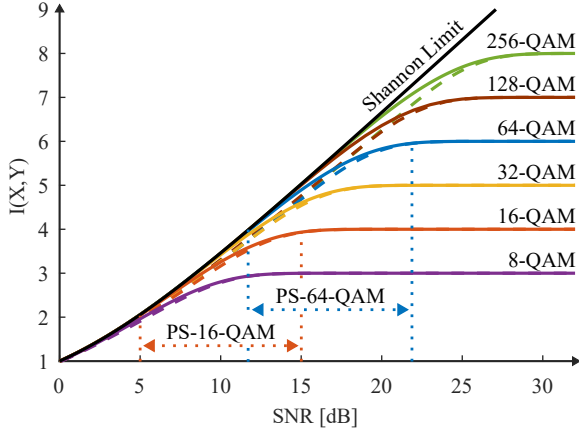


Fig. 1. Achievable mutual information for typical M-QAM modulation formats. Dashed lines: uniform constellation. Solid line: probabilistically shaped constellation. The dotted lines indicate the interval of interest for PS-16-QAM and PS-64-QAM.

where λ is the shaping parameter and M is the constellation size. The choice of λ must be made carefully, as the optimum value varies according to the signal power, modulation format and SNR. Fig. 1 shows the achievable mutual information for typical modulation formats with uniform (dashed line) and shaped (solid line) constellations. For the sake of clarity, we focus in this paper on the PS-16-QAM and PS-64-QAM formats, but the analysis can also be easily extended to other schemes. Fig. 1 helps to understand the range of SNRs for which shaping should be applied for a specific modulation format. For PS-64-QAM, for example, PS should not be applied for SNRs higher than 22 dB, as uniform and shaped constellations achieve the same maximum mutual information. On the other hand, PS should not be deployed with an SNR below 12 dB, as PS-32-QAM achieves equivalent performance using a potentially lower implementation penalty. An analogous analysis can be carried out for the PS-16-QAM modulation format, where the SNR interval of interest ranges from 5 dB to 15 dB. Fig. 2 shows the optimum λ parameter for the PS-16-QAM and PS-64-QAM modulation formats, with in-phase and quadrature components having amplitudes¹ $\pm(2i+1)$, $i = 0, 1, \dots, \sqrt{M}/2 - 1$. The figure allows to infer the range of λ for which PS should be implemented, namely, from 0 to 0.17 for PS-16-QAM and from 0 to 0.05 for PS-64-QAM. Therefore, for the sake of simplicity, we adopted the range from 0 to 0.2 for λ throughout the simulations.

The BPS algorithm estimates the phase noise rotation θ_n as the angle that minimizes the sum of squared distances between N adjacent symbols s_i , rotated by a test phase θ_r , and their respective estimates \hat{s}_i . In this paper we assume an infinite number of test phases and do not delve into resolution issues. In mathematical terms, estimate $\hat{\theta}_n$ is obtained as:

$$\hat{\theta}_n = \min_{\theta_r} J(\theta_r) \quad (3)$$

¹Note that the choice of λ depends on the signal power.

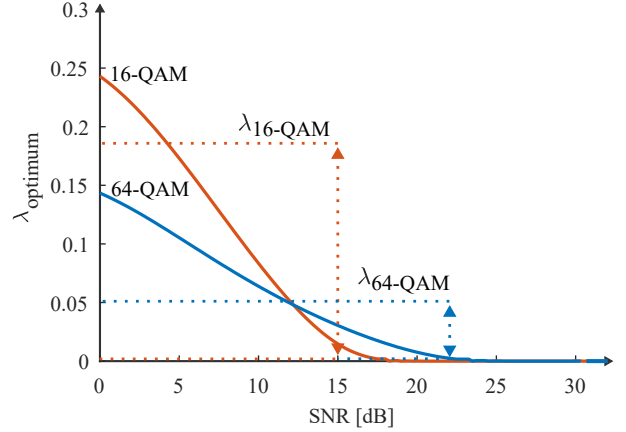


Fig. 2. Optimum values of λ for PS-16-QAM and PS-64-QAM. The dotted lines indicate the range of λ s that corresponds to the interval of interest shown in Figure 1.

where the cost function $J(\theta_r)$ is given by:

$$J(\theta_r) = \sum_{i=1}^N |e^{-j\theta_r}(s_i e^{j\theta_n} + n'_i) - \hat{s}_i|^2 \quad (4)$$

$$= \sum_{i=1}^N |s_i e^{j(\theta_n - \theta_r)} - \hat{s}_i + n_i|^2 \quad (5)$$

Term n_i is a rotated Gaussian process of the same mean and variance of n'_i . It is also possible to write $J(\theta_r)$ as a function of the symbol error $e_i = s_i - \hat{s}_i$:

$$J(\theta_r) = \sum_{i=1}^N |s_i e^{j(\theta_n - \theta_r)} - s_i + e_i + n_i|^2 \quad (6)$$

III. SUPERVISED PHASE SEARCH (SPS)

In this section we introduce the SPS algorithm as an upper bound to the BPS performance. SPS follows the same steps of BPS, except for the fact that the algorithm is not affected by erroneous decisions. In practical implementations, SPS can be deployed in bursts to periodically refresh BPS. In SPS $e_i = 0$ and the analytical modeling is simplified. A geometric analysis of the problem enables us to rewrite (6) as:

$$J(\theta_r) = \sum_{i=1}^N \left[\left(2|s_i| \sin\left(\frac{\theta_n - \theta_r}{2}\right) + n_i^{(1)} \right)^2 + (n_i^{(2)})^2 \right] \quad (7)$$

where $n_i^{(1)}$ is the noise component in the direction of the subtraction of s_i and its rotated version $s_i e^{j(\theta_n - \theta_r)}$, and $n_i^{(2)}$ is the perpendicular component. Both $n_i^{(1)}$ and $n_i^{(2)}$ are zero mean real Gaussian processes with variance σ_n^2 each.

We find $\hat{\theta}_n$ by differentiating $J(\theta_r)$ with respect to θ_r :

$$\frac{dJ(\theta_r)}{d\theta_r} = \sum_{i=1}^N -2 \left(2|s_i| \sin\left(\frac{\theta_n - \theta_r}{2}\right) + n_i^{(1)} \right) |s_i| \cos\left(\frac{\theta_n - \theta_r}{2}\right) \quad (8)$$

Setting the derivative equal to zero, and supposing a small $\theta_n - \hat{\theta}_n$, yields:

$$\sum_{i=1}^N \left(2|s_i| \sin \left(\frac{\theta_n - \hat{\theta}_n}{2} \right) + n_i^{(1)} \right) |s_i| \approx 0 \quad (9)$$

$$\sum_{i=1}^N 2|s_i|^2 \sin \left(\frac{\theta_n - \hat{\theta}_n}{2} \right) + \sum_{i=1}^N (n_i^{(1)}) |s_i| \approx 0 \quad (10)$$

$$\sin \left(\frac{\theta_n - \hat{\theta}_n}{2} \right) \approx -\frac{1}{2} \frac{\sum_{i=1}^N (n_i^{(1)}) |s_i|}{\sum_{i=1}^N |s_i|^2} \quad (11)$$

Approximating $\sin(x) \approx x$, gives:

$$\frac{\theta_n - \hat{\theta}_n}{2} \approx -\frac{1}{2} \frac{\sum_{i=1}^N (n_i^{(1)}) |s_i|}{\sum_{i=1}^N |s_i|^2} \quad (12)$$

$$\hat{\theta}_n \approx \theta_n + \frac{\sum_{i=1}^N (n_i^{(1)}) |s_i|}{\sum_{i=1}^N |s_i|^2} \quad (13)$$

The mean squared error (MSE) in the estimation of θ_n can be obtained as:

$$\text{MSE}(N) = E\{(\theta_n - \hat{\theta}_n)^2\} = E \left\{ \left[\frac{\sum_{i=1}^N (n_i^{(1)}) |s_i|}{\sum_{i=1}^N |s_i|^2} \right]^2 \right\} \quad (14)$$

The computation of (14) is not trivial for intermediate values of N , but the extreme cases offer interesting insights. Setting $N = 1$ gives:

$$\text{MSE}(1) = E \left\{ \left[\frac{n_i^{(1)}}{|s_i|} \right]^2 \right\} = \sigma_n^2 \sum_{m=1}^M \frac{1}{|s_m|^2} P_m \quad (15)$$

Clearly, for small windows the SPS performance depends not only on the SNR, but on the a-priori probability distribution of transmitted symbols. In communications systems with PS implemented by the Maxwell-Boltzmann distribution, it can be shown, by differentiating (15) with respect to λ and setting the result equal to zero, that the MSE is maximized by the following condition:

$$[E\{|s_i|^4\} - 2E\{|s_i|^2\}^2] E \left\{ \left| \frac{1}{s_i} \right|^2 \right\} + E\{|s_i|^2\} = 0 \quad (16)$$

The derivation of (16) is omitted here because of space limitations. By inspection of (16) one can observe that the SPS performance is affected by several moments of $|s_i|$ and $1/|s_i|$, including the fourth central moment of $|s_i|$. For M-QAM constellations, where $E\{s_i^2\} = 0$, it's possible to rewrite (16) in terms of its Kurtosis, given by $K_s = E\{|s_i|^4\} - 2E^2\{|s_i|^2\} - |E\{s_i^2\}|^2$. Thus, the MSE is maximized when:

$$K_s = -\frac{E\{|s_i|^2\}}{E\{|1/s_i|^2\}} \quad (17)$$

On the other hand, supposing a large value of N , called here N_L , the law of large numbers can be invoked to assume that, in the observation window, $N_L P_m$ symbols of type s_m occur. Thus, $\text{MSE}(N_L)$ becomes:

$$\text{MSE}(N_L) \approx \frac{\sigma_n^2 N_L \sum_{m=1}^M |s_m|^2 P_m}{N_L^2 (\sum_{m=1}^M |s_m|^2 P_m)^2} \quad (18)$$

$$= \frac{\sigma_n^2}{N_L (\sum_{m=1}^M |s_m|^2 P_m)} = \frac{\sigma_n^2}{N_L P_s} = \frac{1}{2N_L} \text{SNR}^{-1} \quad (19)$$

where $P_s = E\{|s_i|^2\}$ is the signal power, and $\text{SNR} = P_s/(2\sigma_n^2)$. Thus, for large window sizes, the SPS performance depends on the SNR, but is weakly affected by the transmitted constellation. This can be explained by the sums of N_L independent and identically distributed random variables in (14), allowing us to invoke the Central Limit Theorem.

Fig. 3 shows the MSE of θ_n for SPS. The solid lines indicate analytical predictions, while the symbols correspond to the results produced by Monte Carlo simulations considering 2^{19} symbols. To circumvent resolution issues, 900 test phases are used in phase search algorithms. The results for $\text{SNR} = 25$ dB and $\text{SNR} = 30$ dB were included as a high-SNR reference. Figs. 3a and 3b show the results for the PS-16-QAM modulation format and $N = 1$ and $N = 100$, respectively. The analytical approximation for $N = 1$ exhibits a good agreement with the simulations, with increasing accuracy for higher SNRs. At $N = 100$ the model accuracy is preserved even at lower SNRs. The same behavior is observed for the PS-64-QAM modulation format in Figs. 3c and 3d. As predicted by the analytical model, for $N = 1$ the MSE can increase as a result of shaping compared with the uniform distribution. This problem can be easily alleviated by longer noise-rejecting windows, for which the MSE is practically independent on the modulation format. The figures for $N = 1$ also show the λ parameter value which maximizes the MSE (λ_{max}), obtained analytically by (16).

IV. BLIND PHASE SEARCH (BPS)

In BPS, $e_i \neq 0$, and the analytical modeling becomes challenging because e_i depends on n_i , s_i and θ_r . Therefore, in this section, the analysis is carried out by simulation. To simplify the discussion and the simulation analysis, we assume that shaping changes the a-priori probability of transmitted symbols, but keep their location in the complex plane in $\pm(2i + 1)$, $i = 0, 1, \dots, \sqrt{M}/2 - 1$. This assumption has a direct influence in the choice of λ , as it depends on the constellation amplitudes (although P_m depends only on the SNR). In practice, the absolute values of signal and noise powers are meaningless for the phase recovery algorithm, as only the SNR dictates the transceiver performance.

There are three main processes that influence the interplay of PS and BPS. Firstly, the increase of λ reduces the occurrence of large amplitude symbols, impairing the BPS performance. This occurs because phase deviations are more easily detected in large amplitude symbols. Secondly, shaping reduces the signal power and, maintaining the same SNR, the noise power is also reduced. This noise reduction helps in estimating phase rotations. Thirdly, in BPS decisions are improved with the increase of shaping, also because the noise power decreases. This can be understood by noting that the

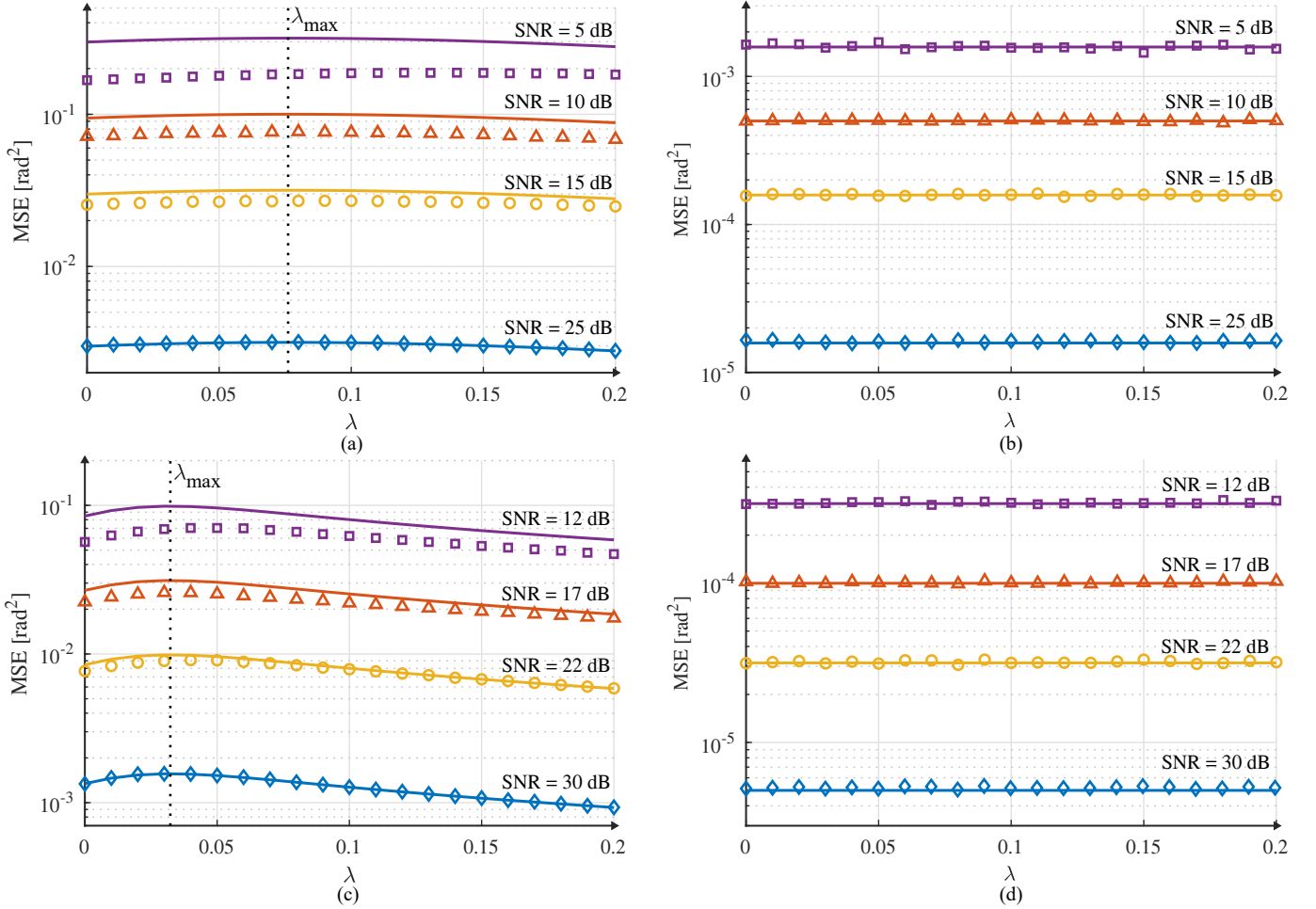


Fig. 3. MSE for SPS with PS-16-QAM and (a) $N = 1$ and (b) $N = 100$. MSE for 64-QAM with (c) $N = 1$ and (d) $N = 100$. The solid lines indicate analytical results obtained by $MSE(1)$ and $MSE(N_L = 100)$, while the symbols were generated by Monte Carlo simulations. The curves indicate that moderate noise-rejecting windows are sufficient to make SPS independent on PS. The vertical dotted lines in figures (a) and (c) indicate λ_{\max} , calculated analytically by (16).

limiting case of shaping of an M-QAM constellation is the QPSK modulation format, which is intrinsically more robust to noise.

Figs 4(a) and 4(b) show the MSE as a function of λ , for BPS evaluated with PS-16-QAM at SNR = 5 dB and with PS-64-QAM at SNR = 12 dB, respectively. Longer noise-rejection windows reduce the MSE, but the filtering gains depend strongly on λ . For example, for the PS-16-QAM format, raising the noise rejecting window from 10 to 500 brings only a 2-fold reduction on the MSE, if the system operates with $\lambda = 0.17$. The same effect can be observed for the 64-QAM format. Without shaping, increasing N from 10 to 100 produces a 10-fold reduction on the MSE. On the other hand, this gain is reduced to 2 if the system operates at $\lambda = 0.05$. It is interesting to note that, for both PS-16-QAM and PS-64-QAM formats, the maximum MSE is achieved near λ_{optimum} , indicating that shaping may pose severe implementation problems to the BPS algorithm. Figs 4(e) and 4(f) show the MSE for BPS evaluated with PS-16-QAM at SNR = 15 dB and with PS-64-QAM at SNR = 22 dB, respectively, which are the highest SNR values for which shaping should be applied. Interestingly, for both conditions

the MSE only decreases with λ , indicating that PS can improve the BPS performance. Figs 4(c) and 4(d) are intermediate cases, where the MSE is evaluated with PS-16-QAM at SNR = 10 dB and with PS-64-QAM at SNR = 17 dB. In all observed cases, λ_{optimum} matches the worst-case condition for BPS. This effect was not present in the SPS analysis, for which a moderate noise-rejecting window was enough to mitigate the impact of PS on the MSE. Therefore, we conjecture that the capacity-maximizing shaping is near to the the worst-case condition for the decision process inside the BPS algorithm.

In addition to the MSE, another meaningful metric to evaluate the impact of phase recovery on the system performance is the symbol error rate (SER). The SER of a square QAM constellation with uniform distribution can be approximated by [14, p. 190]:

$$\text{SER}(\text{SNR}) \approx 4 \left(1 - \frac{1}{\sqrt{M}} \right) Q \left(\frac{3\text{SNR}}{(M-1)} \right) - 4 \left(1 - \frac{1}{\sqrt{M}} \right) Q^2 \left(\frac{3\text{SNR}}{(M-1)} \right) \quad (20)$$

where $Q(\alpha) = \frac{1}{\sqrt{2\pi}} \int_{\alpha}^{\infty} e^{-\frac{x^2}{2}} dx$. For the transmission of

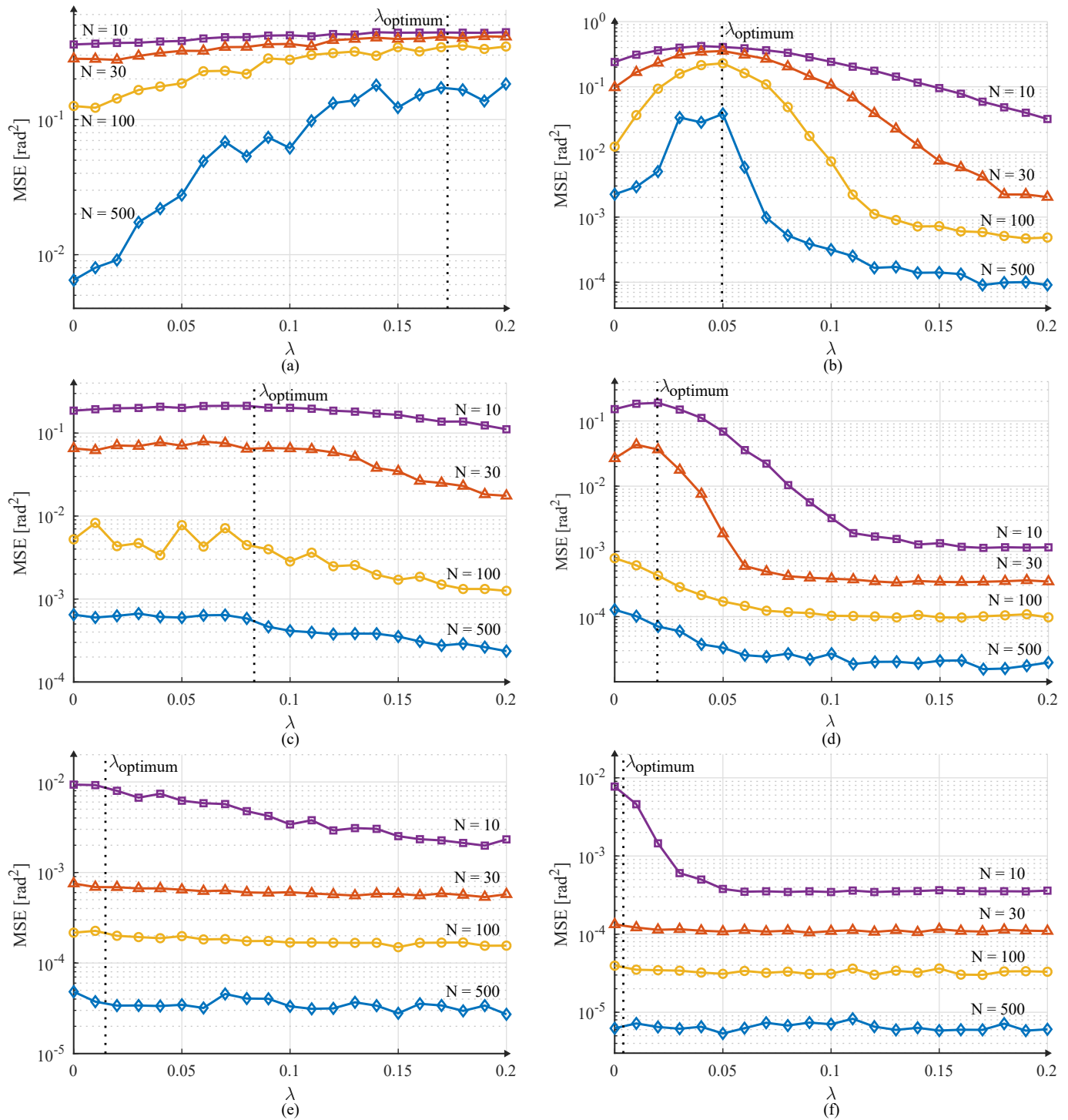


Fig. 4. MSE for BPS with $N = 10, 30, 100,$ and 500 , evaluated with PS-16-QAM at (a) SNR = 5 dB, and (c) SNR = 10 dB, and (e) SNR = 15 dB; and evaluated with PS-64-QAM at (b) SNR = 12 dB, (d) SNR = 17 dB, and (f) SNR = 22 dB. The dotted lines indicate λ_{optimum} for the corresponding configuration.

symbols with unequal a-priori probabilities, a Maximum a Posteriori (MAP) receiver should be used to minimize the SER. However, a MAP decoder adds extra complexity to the phase recovery algorithm, as the a priori probabilities and noise power are required for proper implementation. Thus, we assume in this paper the deployment of a BPS algorithm that uses Maximum Likelihood (ML) detection, whose decision boundaries do not depend on the noise power. To obtain the expression for SER with probabilistic shaping, one can consider a hypothetical condition in which the position of the symbols of the transmitted constellation is kept constant, and only the a-priori probabilities are varied. Note that, in this case, the decision regions of the ML decoder also remain constant. However, to maintain the same SNR of the original constellation without shaping, the noise power should be reduced. Thus, the theoretical SER for shaped transmission (SER_s) can be obtained by adapting (20), using a scaling factor to the SNR to account for the reduction of noise power due to shaping:

$$SER_s(\text{SNR}) = SER(\text{SNR}_s) \quad (21)$$

where the scaled SNR_s is given by:

$$\text{SNR}_s = \text{SNR} \frac{\sum_{m=1}^M |s_m|^2 / M}{\sum_{m=1}^M |s_m|^2 P_m} \quad (22)$$

Note that, for unshaped transmission, $P_m = 1/M$ and $\text{SNR}_s = \text{SNR}$. As PS increases the probability of transmitting lower amplitude symbols, SNR_s increases and SER_s decays.

Figs. 5a and 5b show the SER for the PS-16-QAM and PS-64-QAM formats, respectively. There is a noticeable correlation of the BPS MSE with the SER. In Fig. 5a, although the theoretical SER_s falls sharply with the increase of λ , the simulation curves exhibit only a subtle decay. In Fig. 5b, the curves for $N > 10$ match the theoretical SER_s for $\lambda = 0$, spread for $\lambda \approx \lambda_{\text{optimum}}$, and then join SER_s again for $\lambda \gg \lambda_{\text{optimum}}$. These results indicate that PS may impact BPS in way to severely impair the overall system performance. This impact can be mitigated by the use of extremely high filtering windows (e.g. $N = 500$), whose deployment would increase complexity and require very low linewidth lasers. Analogous effects can be observed in Figs. 5c and 5d, for intermediate SNR values, but in a smaller scale. As shown in Figs. 5e and 5f, PS has a positive effect on BPS at high SNRs, and the SER is not impaired at increasing λ . The high variability at large λ appears because of the low SER achieved in this region, which affects the simulation precision.

V. CONCLUSION

The interplay of PS and the BPS algorithm was investigated analytically and by simulation. We started by analyzing the performance of an SPS algorithm, which has the same architecture of BPS, except for the decision process, which is assumed perfect. We provided an analytical expression for the MSE of SPS, which exhibited a good agreement with simulations. The results demonstrated that PS affects the performance of SPS at short noise-rejecting windows, but this impact is easily mitigated at windows of moderate sizes. At large windows, the SPS MSE is independent on

the modulation format and, thus, insensitive to PS. The BPS algorithm, however, revealed a strong dependence on PS, even for long noise-rejecting windows. Given the differences in behavior of SPS and BPS, we infer that the decisions made inside the BPS algorithm are affected by shaping. For this reason, even long noise rejection windows may provide only modest gains to the algorithm performance. It was also observed, for the simulated scenarios, that the worst shaping condition for the BPS algorithm was near to the capacity-maximizing operation point. Finally, SER simulations showed that the PS impact on BPS can affect the whole transmission performance, specially at low SNR. In this condition, the performance degradation caused by BPS can exceed potential capacity gains expected by PS. This effect can be mitigated by extremely long noise-rejection windows, which increase complexity and require very low linewidth lasers. These finds suggest the need for alternative phase recovery algorithms to be deployed in probabilistically-shaped transmissions.

REFERENCES

- [1] F. A. Barbosa, J. D. Reis, and D. A. A. Mello, "Interplay of probabilistic shaping and the unsupervised blind phase search algorithm," in *Invited, to appear in SPPCOM 2018*, July 2018.
- [2] F. R. Kschischang and S. Pasupathy, "Optimal nonuniform signaling for Gaussian channels," *IEEE Transactions on Information Theory*, vol. 39, no. 3, pp. 913–929, May 1993.
- [3] U. Wachsmann, R. F. H. Fischer, and J. B. Huber, "Multilevel codes: theoretical concepts and practical design rules," *IEEE Transactions on Information Theory*, vol. 45, no. 5, pp. 1361–1391, Jul 1999.
- [4] G. Böcherer, F. Steiner, and P. Schulte, "Bandwidth efficient and rate-matched low-density parity-check coded modulation," *IEEE Transactions on Communications*, vol. 63, no. 12, pp. 4651–4665, Dec 2015.
- [5] L. Beygi, E. Agrell, J. M. Kahn, and M. Karlsson, "Rate-adaptive coded modulation for fiber-optic communications," *Journal of Lightwave Technology*, vol. 32, no. 2, pp. 333–343, Jan 2014.
- [6] D. A. A. Mello, A. N. Barreto, T. C. de Lima, T. F. Portela, L. Beygi, and J. M. Kahn, "Optical networking with variable-code-rate transceivers," *Journal of Lightwave Technology*, vol. 32, no. 2, pp. 257–266, Jan 2014.
- [7] M. P. Yankov, D. Zibar, K. J. Larsen, L. P. B. Christensen, and S. Forchhammer, "Constellation shaping for fiber-optic channels with QAM and high spectral efficiency," *IEEE Photonics Technology Letters*, vol. 26, no. 23, pp. 2407–2410, Dec 2014.
- [8] T. Fehenberger, G. Böcherer, A. Alvarado, and N. Hanik, "LDPC coded modulation with probabilistic shaping for optical fiber systems," in *2015 Optical Fiber Communications Conference and Exhibition (OFC)*, March 2015, pp. 1–3.
- [9] F. Buchali, G. Böcherer, W. Idler, L. Schmalen, P. Schulte, and F. Steiner, "Experimental demonstration of capacity increase and rate-adaptation by probabilistically shaped 64-QAM," in *2015 European Conference on Optical Communication (ECOC)*, Sept 2015.
- [10] O. D. Domingues, D. A. A. Mello, R. da Silva, S. Ark, and J. M. Kahn, "Achievable rates of space-division multiplexed submarine links subject to nonlinearities and power feed constraints," *Journal of Lightwave Technology*, vol. 35, no. 18, pp. 4004–4010, Sept 2017.
- [11] A. Ghazisaeidi, I. F. d. Jauregui Ruiz, R. Rios-Muller, L. Schmalen, P. Tran, P. Brindel, A. C. Meseguer, Q. Hu, F. Buchali, G. Charlet, and J. Renaudier, "65Tb/s transoceanic transmission using probabilistically-shaped PDM-64QAM," in *ECOC 2016 - Post Deadline Paper; 42nd European Conference on Optical Communication*, Sept 2016.
- [12] J. Renner, T. Fehenberger, M. P. Yankov, F. D. Ros, S. Forchhammer, G. Bcherer, and N. Hanik, "Experimental comparison of probabilistic shaping methods for unrepeatable fiber transmission," *Journal of Lightwave Technology*, vol. 35, no. 22, pp. 4871–4879, Nov 2017.
- [13] D. Piloni, L. Bertignono, A. Nespola, F. Forghieri, and G. Bosco, "Comparison of probabilistically shaped 64QAM with lower cardinality uniform constellations in long-haul optical systems," *Journal of Lightwave Technology*, vol. 36, no. 2, pp. 501–509, Jan 2018.
- [14] J. R. Barry, E. A. Lee, and D. G. Messerschmitt, *Digital Communication*, 3rd ed. Kluwer Academic Publishers, 2004.

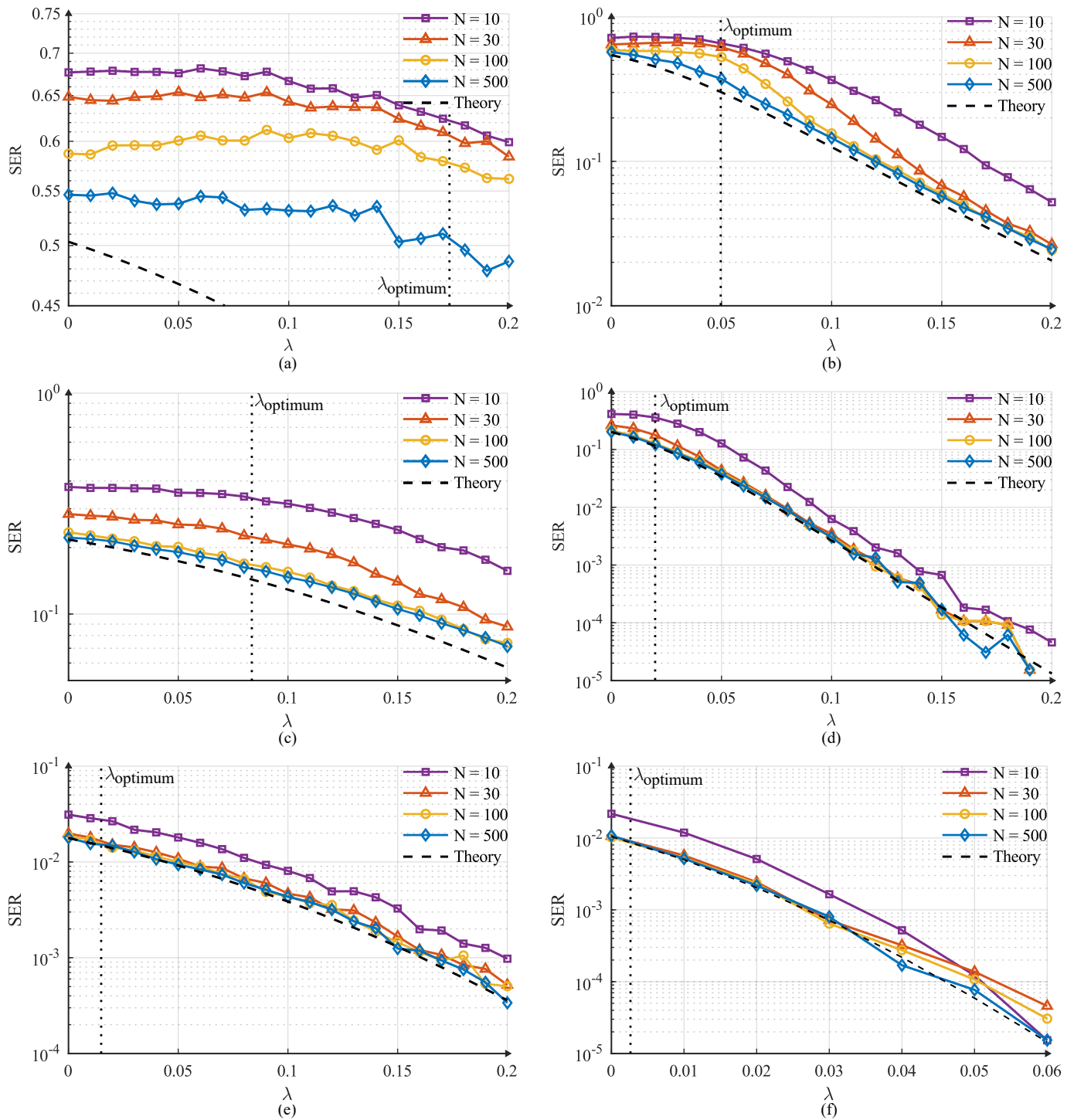


Fig. 5. SER for BPS with $N = 10, 30, 100,$ and 500 , evaluated with PS-16-QAM at (a) SNR = 5 dB, and (c) SNR = 10 dB, and (e) SNR = 15 dB; and evaluated with PS-64-QAM at (b) SNR = 12 dB, (d) SNR = 17 dB, and (f) SNR = 22 dB.